

The effect of the molecular structures of dicyanomethylene compounds on their supramolecular assembly, photophysical and electrochemical properties†

Cite this: *Phys. Chem. Chem. Phys.*, 2013, **15**, 13013

Catiúcia R. M. O. Matos,^a Fabio S. Miranda,^a José W. de M. Carneiro,^a Carlos B. Pinheiro^b and Célia M. Ronconi^{*a}

Two series of flexible dicyanomethylene compounds, specifically, *class 1* and *class 2* compounds, have been designed and synthesised. In *class 1* compounds, the dicyanomethylene groups are separated by glycol chain spacers of different lengths, whereas, in *class 2* compounds, the spacers are alkyl linkers of different lengths. The notion underlying the design of these compounds is that in *class 1* molecules, the spacers contain donor oxygen atoms that could not only form hydrogen bonds during the course of crystal packing but also promote withdrawing effects that modify the photophysical and electrochemical properties of these molecules in solution; in contrast, these effects would be absent for *class 2* molecules. However, this study revealed that, with respect to crystal packing, the size of the spacers and their even and odd numbers of atoms are more important than their chemical nature. All of the synthesised compounds exhibited blue emission in the solid state and in CH₂Cl₂ solutions. The photophysical and electrochemical properties of these compounds in solution were not significantly affected by the type and length of the spacer that was used in each molecule. In the solid state, however, the compound with the shortest spacer showed the highest Stokes shift. The electronic transitions for the synthesised compounds in solution were explained by density functional theory and time-dependent density functional theory calculations, which indicated that the methylene moieties control the properties of both classes of compounds and that the spacers do not conjugate with the end groups. These two series of flexible dicyanomethylene compounds could be utilised as molecular building blocks for the development of new solids with novel properties.

Received 8th May 2013,
Accepted 31st May 2013

DOI: 10.1039/c3cp51957k

www.rsc.org/pccp

Introduction

The crystal engineering of new structures with target properties is a challenging research area in modern chemistry.¹ In the field of coordination chemistry, particularly with respect to the study of coordination polymers, the design and preparation of molecular building blocks (MMBs) with covalent frameworks that incorporate the capacity to achieve a directed connectivity between subunits for the assembly of supramolecular structures is the key approach for obtaining desired structures and functions.^{2,3}

In principle, the introduction of chemically or electrostatically active regions into organic ligands can govern the formation of supramolecular arrays. Several strategies to obtain predetermined ordered structures have been developed, such as the directional-bond approach,^{4,5} the symmetry interaction model^{6,7} and methods that utilise reticular chemistry.⁸ These strategies typically function best if rigid ligands and preferred coordination motifs of the metal cations are used to improve the predictability of supramolecular structures.⁸ However, in practice, many subtle considerations, such as the solvent system,⁹ the temperature,¹⁰ the nature of the counter anions,¹¹ the coordination properties of the metal cations¹² and the functionality of the ligands¹³ can also affect the self-assembly of these supramolecular architectures.

The structures formed between flexible ligands and metals are less predictable than the structures produced between rigid ligands and metals because of the conformational freedom of flexible ligands.^{10,14} Polydentate flexible ligands have been extensively used for the construction of polynuclear compounds

^a Instituto de Química, Universidade Federal Fluminense, Campus do Valonguinho, CEP 24020-141, Niterói, RJ, Brazil. E-mail: cmronconi@id.uff.br; Fax: +55 21 26292136; Tel: +55 21 26292164

^b Departamento de Física, ICEX, Universidade Federal de Minas Gerais, Av. Antônio Carlos, 6627 Pampulha, CEP 31270-901, Belo Horizonte, MG, Brazil

† Electronic supplementary information (ESI) available. CCDC 908002–908004 and 929360. For ESI and crystallographic data in CIF or other electronic format see DOI: 10.1039/c3cp51957k

and for the transmission of magnetic exchanges because of their versatile coordination modes and conformations.^{15,16} Therefore, one interesting research direction involves attempting to achieve a better understanding of the ways in which the molecular properties of flexible ligands can affect the supramolecular structures and properties of compounds.

To obtain insights into this topic, we have synthesised a series of flexible dicyanomethylene compounds and have investigated their crystallisation and optical properties in the solid state and in solution. This study was conducted in an effort to understand their supramolecular assembly in the solid state and the relationship with their photophysical properties in both solid state and solution. This understanding will be applied to the design of new solids with desirable physical and chemical properties. The synthesised compounds include in their structural components: (i) two dicyanomethylene moieties that are symmetrically distributed on the molecule and separated by (ii) highly flexible $(-\text{CH}_2\text{OCH}_2-)_n$ or $(-\text{CH}_2\text{CH}_2-)_n$ spacers of different lengths. The dicyanomethylene groups are interesting because they can act as π -acceptors and also present remarkable coordination properties which make these compounds potentially useful in the field of coordination polymers.^{10,17–19} The oxygen atom in the ligands that contain glycol spacers can also behave as a donor atom in the formation of hydrogen bonds. The compounds with glycol chain spacers of different lengths will be referred to as *class 1* compounds whereas in *class 2* compounds, the spacers are alkyl linkers of different lengths. All of the synthesised compounds have interesting photochemical and electrochemical properties. We also discuss a detailed theoretical investigation of the electronic properties in the ground and excited states that utilises density functional theory (DFT) and time-dependent DFT (TD-DFT).

Results and discussion

Synthesis

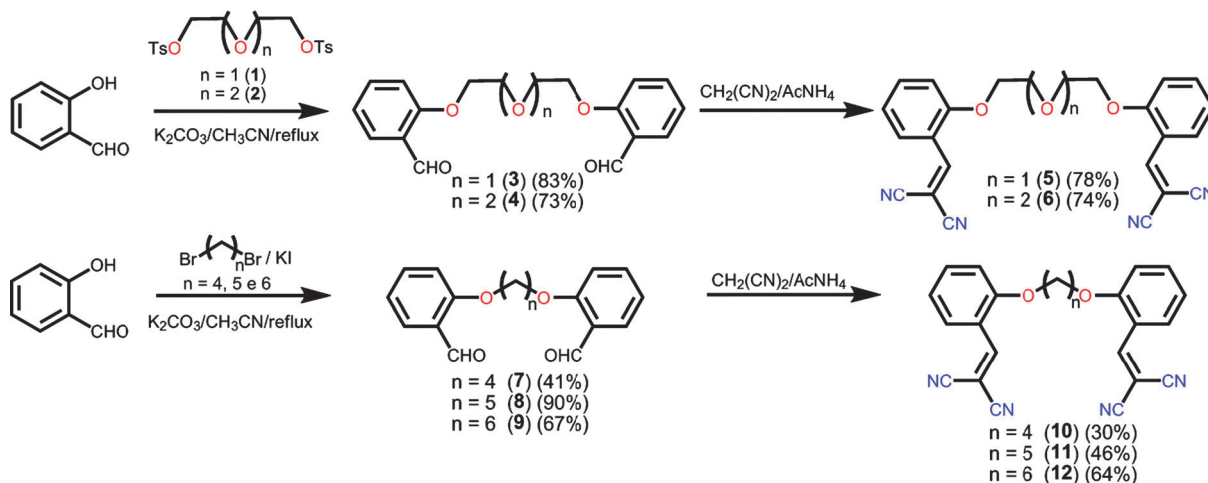
The synthetic routes for obtaining compounds **5**, **6**, **10**, **11** and **12** and their intermediates **3**, **4**, **7**, **8** and **9** are outlined in

Scheme 1. Compounds **3** and **4** were obtained through the reaction of 1 equiv. of the appropriate bis-tosylate with 2 equiv. of salicylic aldehyde in dry MeCN in the presence of K_2CO_3 . Compounds **7**, **8** and **9** were obtained through the addition of 1 equiv. of dibromoalkanes to 2 equiv. of salicylic aldehyde in dry MeCN in the presence of K_2CO_3 . Addition of dinitriles to the dialdehydes in the presence of NH_4OAc by mechanochemical reactions, without solvent, yielded compounds **5**, **6**, **10**, **11** and **12** as yellow crystalline powders. The compounds were fully characterised through both ^1H and ^{13}C nuclear magnetic resonance (NMR), Fourier transform infrared (FTIR) spectroscopy (see ESI,† Fig. S1–S15) and elemental analysis.

X-ray crystallography

X-ray diffraction measurements were performed on compounds **5**, **6**, **10**, **11** and **12** at temperatures indicated in Table 1. For compounds **5**, **10**, **11** and **12**, data collection and structure refinement processes of the X-ray diffraction experiments are summarised in Table 1. Compound **6** provided single crystals of poor quality and X-ray diffraction data were used only to identify its molecular shape.

Compounds **5** and **11** possess the same number of atoms (seven) in their spacers; compound **5** contains one oxygen atom in the middle of its spacer, whereas compound **11** contains a carbon atom at this location. In principle, this extra oxygen atom in compound **5** could serve as a donor atom to form hydrogen bonds. However, **5** and **11** crystallize in the same space group, $P2_1/c$, and both possess the same molecular geometry and crystal packing as evidenced by the juxtaposition of the structures (see ESI,† Fig. S16). In both compounds, the three-dimensional packing involves three different kinds of hydrogen-bond-like short contacts, $\text{C-H}\cdots\text{N}$, labelled **I**, **II** and **III** (Fig. 1 and Table 2; see also ESI,† Fig. S17). The short contact **I** involves the hydrogen atom of the methylene group and the N atom of the cyano group. Interaction **I** regulates compounds **5** and **11** into end-to-end assemblies. In the short contact **II**, the hydrogen atom of the benzene ring carbon and N atom of the cyano group are involved. Finally, the short contact **III** arises from an electrostatic interaction between the N atom of the



Scheme 1 The synthesis of dicyanomethylene compounds.

Table 1 Crystallographic data and structure refinement

Identification code	5	10	11	12
Empirical formula	C ₂₄ H ₁₈ N ₄ O ₃	C ₁₂ H ₉ N ₂ O	C ₂₅ H ₂₀ N ₄ O ₂	C ₂₆ H ₂₂ N ₄ O ₂
Formula weight	410.42	197.21	412.48	422.48
Temperature (K)	123(2)	140(2)	293(2)	120(2)
Wavelength (Å)	1.54178	0.71073	0.71073	0.71073
Crystal system, space group	Monoclinic, <i>P2/c</i>	Triclinic, <i>P</i> $\bar{1}$	Monoclinic, <i>P2/c</i>	Monoclinic, <i>P2₁/n</i>
Unit cell dimensions (Å, °)	<i>a</i> = 27.6303(10), <i>b</i> = 4.1076(2), <i>c</i> = 19.1097(6), β = 110.163(3)	<i>a</i> = 4.1838(3), <i>b</i> = 9.5667(6), <i>c</i> = 12.2486(8), α = 96.676(5), β = 91.076(5), γ = 93.139(6)	<i>a</i> = 27.4442(16), <i>b</i> = 4.3997(3), <i>c</i> = 19.1278(12), β = 110.361(6)	<i>a</i> = 4.3137(2), <i>b</i> = 9.9807(4), β = 94.618(3), <i>c</i> = 25.5817(8)
Volume (Å ³)	2035.92(14)	486.04(6)	2165.3(2)	1097.81(8)
Z, calculated density (Mg m ⁻³)	4, 1.339	2, 1.348	4, 1.265	2, 1.278
Absorption coefficient (mm ⁻¹)	0.741	0.089	0.082	0.083
<i>F</i> (000)	856	206	872	444
Crystal size (mm)	0.45 × 0.15 × 0.10	0.61 × 0.27 × 0.10	0.64 × 0.21 × 0.10	0.48 × 0.38 × 0.15
θ range for data collection (°)	2.46 to 66.61	2.15 to 26.37	2.97 to 25.19	2.19 to 26.37
Limiting indices	-32 ≤ <i>h</i> ≤ 31; -4 ≤ <i>k</i> ≤ 4; -22 ≤ <i>l</i> ≤ 22	5 ≤ <i>h</i> ≤ 5, -11 ≤ <i>k</i> ≤ 10, -15 ≤ <i>l</i> ≤ 15	-32 ≤ <i>h</i> ≤ 32; -4 ≤ <i>k</i> ≤ 5; -22 ≤ <i>l</i> ≤ 21	-5 ≤ <i>h</i> ≤ 5; -12 ≤ <i>k</i> ≤ 12; -31 ≤ <i>l</i> ≤ 31
Reflections collected/independent	22 251/3559, [<i>R</i> (int) = 0.0336]	5801/1985, [<i>R</i> (int) = 0.0381]	15 433/3447, [<i>R</i> (int) = 0.0569]	17 312/2259, [<i>R</i> (int) = 0.0247]
Completeness	(θ_{\max} = 66.61°), 99.5%	(θ_{\max} = 26.37°), 99.7%	(θ_{\max} = 25.19°), 88.1%	(θ_{\max} = 26.37°), 100.0%
Max. and min. transmission	1.00 and 0.860	0.993 and 0.970	0.990 and 0.954	0.988 and 0.964
Refinement method	Full-matrix least-squares on <i>F</i> ²	Full-matrix least-squares on <i>F</i> ²	Full-matrix least-squares on <i>F</i> ²	Full-matrix least-squares on <i>F</i> ²
Data/restraints/parameters	3559/0/282	1985/0/136	3447/0/282	2259/0/145
Goodness-of-fit on <i>F</i> ²	1.065	1.057	1.030	1.039
Final <i>R</i> indices [<i>I</i> > 2σ(<i>I</i>)]	<i>R</i> ₁ = 0.0434, <i>wR</i> ₂ = 0.1136	<i>R</i> ₁ = 0.0464, <i>wR</i> ₂ = 0.1126	<i>R</i> ₁ = 0.0556, <i>wR</i> ₂ = 0.1366	<i>R</i> ₁ = 0.0366, <i>wR</i> ₂ = 0.0916
<i>R</i> indices (all data)	<i>R</i> ₁ = 0.0441, <i>wR</i> ₂ = 0.1151	<i>R</i> ₁ = 0.0678, <i>wR</i> ₂ = 0.1303	<i>R</i> ₁ = 0.0792, <i>wR</i> ₂ = 0.1550	<i>R</i> ₁ = 0.0400, <i>wR</i> ₂ = 0.0942

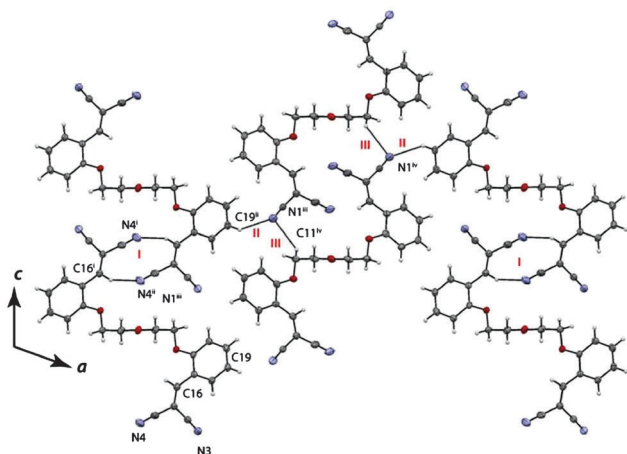


Fig. 1 Representation of the crystal packing of compound **5**. Oxygen atoms are indicated in red and nitrogen in blue. Displacement ellipsoid parameters are drawn at the 50% probability level. Symmetry codes (i) $-x + 1, -y, -z + 1$; (ii) $x, 1 - y, 0.5 + z$; (iii) $x, 2 - y, 0.5 + z$; (iv) $x, 1 + y, z$.

cyano group and the hydrogen atom of the carbon adjacent to the oxygen atom of the spacer.

The electrostatic potential surfaces were obtained for all compounds (see ESI,† Fig. S18). The charge distribution in the dicyanomethylene compounds showed that the nitrogen atoms from the cyano groups are negatively charged, as expected, and the hydrogen atoms adjacent to the oxygen atoms in the spacers are positively charged, showing that these atoms can electrostatically interact as observed in Fig. 1–3.

Table 2 Short contacts [measured in Å and °]

Compounds	D–H...A ^a	<i>d</i> (D–H)	<i>d</i> (H...A)	<i>d</i> (D...A)	Angle (DHA)	Type of inter-action
5	C4–H4...N2 ⁱ	0.95	2.53	3.413(3)	154.2	I
	C16–H16...N4 ⁱⁱ	0.95	2.51	3.389(3)	153.1	I
	C19–H19...N1 ⁱⁱⁱ	0.95	2.58	3.402(3)	144.5	II
	C11–H11B...N1 ^{iv}	0.99	2.74	3.493(3)	132.8	III
10	C4–H4...N2 ^v	0.95	2.64	3.545(2)	158.4	I
	C11–H11A...N1 ^{vi}	0.99	2.70	3.491(2)	137.5	III
11	C4–H4...N2 ⁱ	0.93	2.64	3.502(6)	154.4	I
	C16–H16...N4 ⁱⁱ	0.93	2.61	3.459(5)	151.7	I
	C19–H19...N1 ⁱⁱⁱ	0.93	2.63	3.436(6)	145.1	II
12	C11–H11b...N1 ^{iv}	0.97	2.77	3.607(6)	144.7	III
	C12–H12B...N2 ^{vii}	0.99	2.60	3.434(2)	141.4	III

^a The following symmetry transformations were used to generate equivalent atoms: (i) $-x + 1, -y, -z + 1$; (ii) $-x, -y + 1, -z$; (iii) $x, y - 1, z$; (vi) $x, 1 - y, 0.5 - z$; (v) $-x - 1, -y + 1, 1 - z + 1$; (vi) $x - 1, y - 1, z$ and (vii) $-x + 1, -y + 1, -z$.

Compound **10** crystallises in a triclinic *P* $\bar{1}$ space group. The unit cell has a volume that is a quarter of that of the unit cells of **5** and **11**. The three-dimensional packing involves the short contacts **I** and **III** (Fig. 2 and Table 2).

Compound **12** crystallises in the monoclinic space group *P2₁/n*. The unit cell has a volume that is half that of the unit cells for **5** and **11**. A number of short electrostatic contacts, namely **III**, and phenyl-ring π -stacking are responsible for the 3D packing of compound **12** (Fig. 3 and Table 2).

A comparison of the structures of compounds **5**, **6**, **10**, **11** and **12** (Fig. 4) reveals a V-shaped arrangement of the phenyl

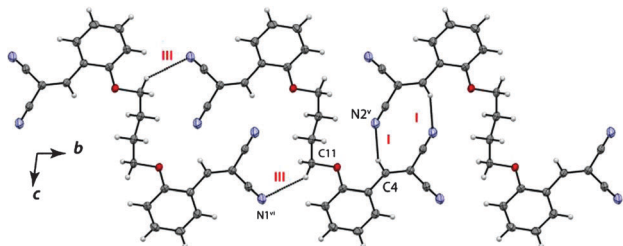


Fig. 2 Representation of the crystal packing of compound **10**. Oxygen atoms are indicated in red and nitrogen in blue. Displacement ellipsoid parameters are drawn at the 50% probability level. Symmetry codes (v) = $-x - 1, -y + 1, 1 - z + 1$; (vi) = $x - 1, y - 1, z$.

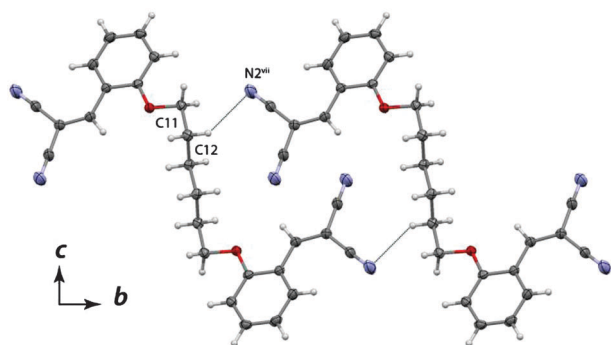


Fig. 3 Representation of the crystal packing of compound **12**. Oxygen atoms are indicated in red. Displacement ellipsoid parameters are drawn at the 50% probability level. Symmetry codes (vii) = $-x + 1, -y + 1, -z$.

rings for the compounds containing an odd number of atoms in the spacer (**5** and **11**) and a parallel arrangement of the phenyl rings for the compounds containing an even number of atoms in the spacer (**6**, **10** and **12**). The angle between the normal vectors of the least square planes defining the aromatic rings in **5** and **11** is approximately 121° and 114° , respectively. Interestingly, the distances between the parallel phenyl rings are 1, 3 and 5 Å for compounds **6**, **10** and **12**, respectively.

Based on these results, it is likely that the size and also the even and odd number of atoms in the spacers are more relevant for the conformations of the dicyanomethylene compounds than the spacers' chemical composition.²⁰

Photophysical properties in the solid state

Normalised diffuse reflectance UV-Vis and photoluminescence spectra of compounds **5**, **6**, **10**, **11** and **12** in the solid state at room temperature are presented in Fig. 5. The photophysical data for these compounds in the solid state are summarised in Table 3. Two absorption bands were observed for all of the examined compounds. The absorption at high wavelength is slightly red shifted for compounds **11** and **12** (*class 2*). To obtain the precise bandgap values from absorption edges, the inflection point in the first derivatives of the absorption spectra was used.²¹ The bandgap values are similar for all of the examined compounds, indicating that the different types of spacers and crystal packing do not significantly affect the bandgap size.

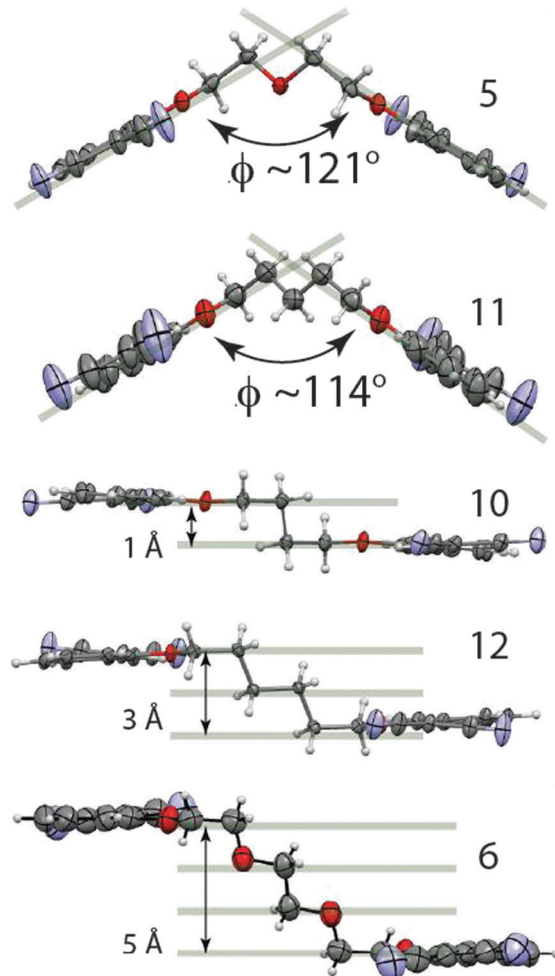


Fig. 4 The conformations of compounds **5**, **6**, **10**, **11** and **12**. Oxygen atoms are indicated in red and nitrogen atoms are represented in blue. Atomic displacement parameters are represented at 50% of probability. ϕ angles are defined as the angle between the normal vectors of the least square planes defining the aromatic rings.

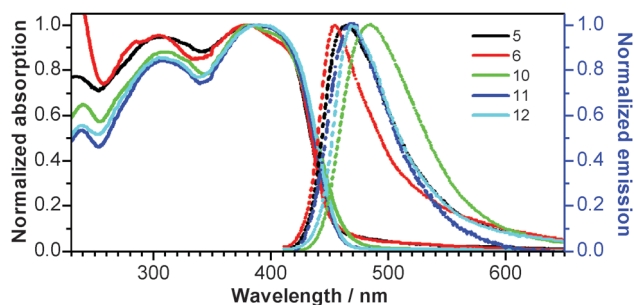


Fig. 5 Normalised absorption (full lines) and emission spectra (dashed lines) of the examined dicyanomethylene compounds, measured in solid state.

The compounds are highly fluorescent in the solid state. Greenish-blue emissions were observed upon irradiation of the solids at the absorption maximum $\lambda_{\text{max}}(2)$ (Table 3). The emission maximum is blue shifted for *class 1* (**5** and **6**) relative to *class 2* compounds (**10**, **11** and **12**). Compound **10** exhibits

Table 3 Optical properties of the dicyanomethylene compounds in the solid state

Compounds	$\lambda_{\max}(1)/$ nm	$\lambda_{\max}(2)/$ nm	$\lambda_{\text{em}}^a/$ nm	Stokes shift/eV	Bandgap ^{b/} eV
5	307	382	465	0.58	2.69
6	303	380	454	0.53	2.68
10	310	382	483	0.68	2.62
11	311	388	470	0.56	2.67
12	312	392	468	0.51	2.67

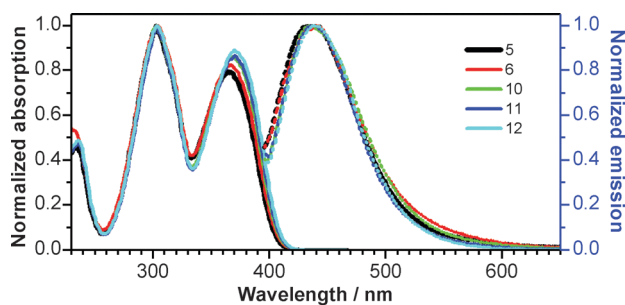
^a Excited at $\lambda_{\max}(2)$. ^b Estimated from the optical absorption edge.

the largest Stokes shift in the series. This compound might be experiencing a larger geometry change upon excitation. A comparison of the crystal structures of all compounds (Fig. 1–3 and Tables 1 and 2) shows that the crystal packing of compound **10** involves two types of short contacts (Table 2), whereas the compounds **5**, **11** and **12** have additional weak interactions such as, phenyl-ring π -stacking (compound **12**) and hydrogen-bond-like short contacts (type **III** in compounds **5** and **11**). These additional weak interactions in compounds **5**, **11** and **12** may cooperatively increase the structural rigidity in the solid state, leading to a smaller Stokes shift for these compounds than for compound **10**.

To gain further insight into the photophysical process within the five examined compounds, we also investigated their absorption and emission behaviour in solution (CH_2Cl_2).

Photophysical properties in solution

Normalised absorption and photoluminescence spectra of compounds **5**, **6**, **10**, **11** and **12** in CH_2Cl_2 solution at room temperature are presented in Fig. 6. Two absorption bands were

**Fig. 6** Normalised absorption (full lines) and emission spectra (dashed lines) of the examined dicyanomethylene compounds, measured in CH_2Cl_2 solutions.**Table 4** Optical and electrochemical properties of the dicyanomethylene compounds in CH_2Cl_2

Compounds	$\lambda_{\max}(1)/$ nm	$\epsilon_1/$ $10^4 \text{ M}^{-1} \text{ cm}^{-1}$	$\lambda_{\max}(2)/$ nm	$\epsilon_2/$ $10^4 \text{ M}^{-1} \text{ cm}^{-1}$	Φ	$\lambda_{\text{em}}/\text{nm}$	$\Delta\lambda^a/\text{eV}$	τ_s/ns	$E_{\text{red}}/\text{V vs.}$ Ag/AgCl	HOMO ^{b/} eV	LUMO ^{c/} eV	Gap _{opt} ^{d/} eV
5	303	3.01	365	2.47	0.02	440	0.58	5.6	-1.17	-6.81	-3.63	3.18
6	303	1.95	366	1.60	0.06	441	0.58	6.1	-1.17	-6.81	-3.63	3.18
10	303	3.02	369	2.64	0.04	436	0.52	5.8	-1.22	-6.76	-3.58	3.18
11	303	2.82	369	2.50	0.03	436	0.52	5.8	-1.16	-6.81	-3.65	3.16
12	303	2.64	371	2.35	0.03	439	0.52	5.8	-1.19	-6.75	-3.61	3.14

^a The Stokes shift. ^b HOMO = LUMO_{elec.} - gap_{opt.} ^c Calculated from the irreversible reduction process. ^d Estimated from the optical absorption edge. The inflection point in the first derivatives of the absorption spectrum was used.

also observed for all of the examined compounds in solution: one at approximately 303 nm and the other near the visible region at ca. 368 nm. The observed molar extinction coefficients for these peaks range from 19 500 to 30 100 and from 16 000 to 26 400 $\text{mol}^{-1} \text{ L}^{-1} \text{ cm}^{-1}$, respectively (Table 4). The primary feature of these spectra is a slight blue shift observed for *class 1* compounds (**5** and **6**) relative to *class 2* compounds (**10**, **11** and **12**). The LUMO/HOMO energy gap was estimated from the absorption edge of the optical absorption spectra (Table 4).^{21,22}

All compounds exhibit blue emissions in CH_2Cl_2 when excited at the absorption maximum $\lambda_{\max}(2)$ (Table 4). Among the examined molecules, compound **6** exhibited the highest quantum yield and fluorescence lifetime ($\Phi = 0.06$ and $\tau_s = 6.1 \text{ ns}$; Table 4). In contrast to the absorption spectra, the emission maximum is blue shifted for *class 2* compounds relative to that of *class 1* compounds. Inversely, in the solid state, the emission maximum was blue shifted for *class 1*. The Stokes shifts of the compounds in solution were 0.58 and 0.52 eV for *class 1* and *2*, respectively. *Class 1* molecules exhibited larger Stokes shifts than *class 2* molecules; behaviour that is not observed in the solid state (Table 3). The larger Stokes shifts for *class 1* compounds in solution may be related to the fact that, relative to *class 2* molecules, *class 1* molecules may display better reorganisation of their excited states because of the withdrawing effects of the glycol spacers. The larger Stokes shifts for *class 1* can also arise from different solvation of the excited state relative to the ground state.²³

Electrochemical properties

Cyclic voltammetry (CV) (see ESI,† Fig. S19) was used to identify the electrochemical behaviour and also to obtain HOMO/LUMO energies of the dicyanomethylene compounds in solution (Table 4). The experiments were performed in argon-purged $\text{CH}_2\text{Cl}_2/\text{TBAClO}_4$, at room temperature. The cyclic voltammograms were obtained in the potential range of +1.00 to -1.50 V vs. Ag/AgCl (in organic medium) quasi-reference electrode. For all of the examined compounds, the potential was scanned from the open-circuit potential. The onsets were referenced to Fc/Fc^+ .^{24,25} The reduction potentials, the electron affinity (EA) (LUMO level), the ionisation energy (IE) (HOMO level) and the optical gap for these compounds are presented in Table 4. The LUMO level was determined using the $E_{\text{LUMO}} = -4.8 - E_{\text{red}}$ (vs. SCE) equation.^{26–31} The HOMO energy levels of all of these compounds were calculated by subtracting the optical gap from the electrochemical LUMO levels (Table 4).

All of the examined compounds are characterised by an irreversible cathodic reduction process that is slightly shifted to more negative potentials for compounds **10** and **12** (which are both *class 2* compounds) relative to the potentials of compounds **5**, **6**, and **11** (see ESI,† Fig. S19). An irreversible anodic oxidation process that occurs after the reduction process is also observed for all of the examined compounds. This anodic oxidation may be related to the oxidation of the reduced product that has been adsorbed onto the surface of the working electrode.

Theoretical calculations

To better understand the photophysical properties of the newly synthesised dicyanomethylene compounds, density functional theory (DFT) was used to perform theoretical calculations at the B3LYP/6-31G(d,p) level.^{32,33} Two sets of geometries were optimized for each compound: (i) one starting from the CIF files obtained from the X-ray diffraction experiments and (ii) the other one with a fully planar geometry in a zig-zag arrangement of the spacers. Relative energies for the two sets of structures are given in Table S1 (ESI†). Considering the final free energy in solution (ΔG_{sol}), the relative energies are below 2 kcal mol⁻¹. The structures obtained from the CIF files for *class 1* compounds (compounds **5** and **6**) are more stable than the planar structures (see ESI,† Table S1). In contrast, the planar arrangements are more stable for *class 2* compounds (**10**, **11** and **12**) (see ESI,† Table S1). Considering the low energy differences between the two sets of structures, in the following analysis only the structures obtained from the X-ray experiments will be discussed.

To assign the absorption bands observed in the UV-Vis spectra, we calculated the molecular orbitals of the compounds in CH₂Cl₂. Fig. 7 displays the contour plots of the frontier orbitals (HOMOs and LUMOs) and their corresponding energy levels and gaps. The HOMOs have π -symmetry and reside mainly on the aromatic rings, whereas the LUMOs have higher amplitude on the double bonds conjugated to the aromatic rings. The conjugation patterns of the

HOMOs involve the O₁₁ atom and one of the e_{1g} orbitals of the benzyl ring, whereas the LUMOs involve mainly the C₇–C₈ double bonds (Fig. 7). Although these calculations were performed in CH₂Cl₂, the same orbitals may be involved in the electronic transitions observed in the solid state absorption spectra (Fig. 5), because the spectra in solution and in solid state are similar.

The theoretical absorption spectra calculated for both the experimental (obtained from CIF files) and the planar structures show a systematic underestimation of the excitation energies (see ESI,† Fig. S20–S24), a result that can possibly be attributed to the limitation of TD-DFT methods for calculation of excitation energies of charge-transfer excited states.^{34,35} In spite of this limitation, the important features of the spectra were correctly simulated. To our present discussion this is adequate, as the TD-DFT calculation has been used mainly to assign the electronic transitions observed in the experimental spectra^{36,37} (see ESI,† Fig. S20–S24 and Tables S5 and S6), rather than to calculate the excitation energies.

The natural transition orbitals (NTOs)³⁸ involved in the electronic transitions of compound **6** are presented in Fig. 8. These calculations were performed only for this compound because the absorption and emission spectra of all of the examined compounds exhibit similar patterns (Fig. 6).

The NTOs are similar to the previously discussed canonical orbitals and feature the same distribution pattern as the canonical orbitals. The NTOs are also associated with either the aromatic system or the adjacent unsaturated group. Thus, the two transitions in the absorption spectra are due to π – π^* electron transfer from the aromatic ring to the unsaturated group. For the excitation at low energies (Fig. 8), which involves transitions from the HOMO and HOMO – 1 orbitals, there is no amplitude on the C₇ carbon (atom labels are shown at the top of Fig. 7).

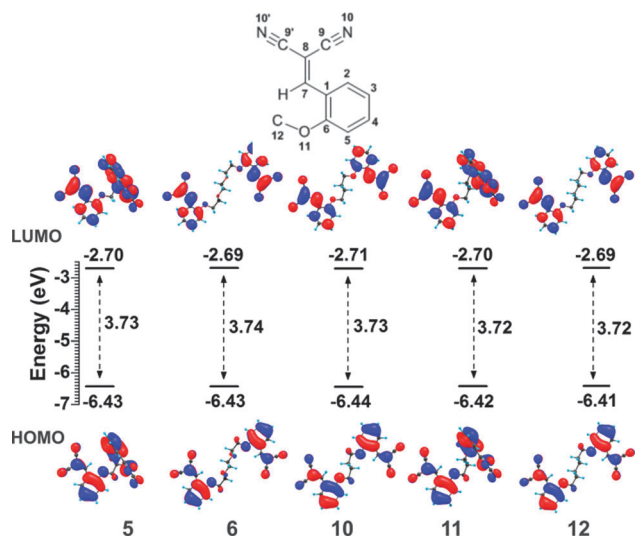


Fig. 7 Calculated HOMOs, LUMOs, energy levels and gaps for the synthesised dicyanomethylene compounds.

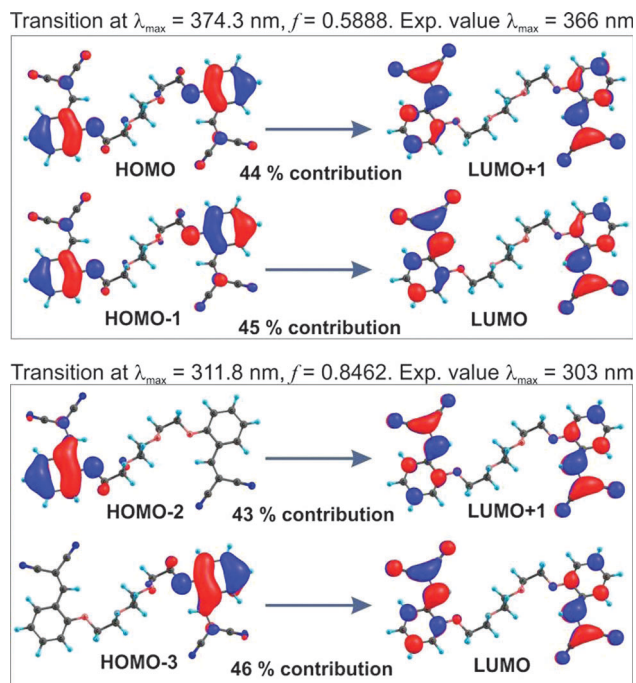


Fig. 8 The NTO contours (isosurface = 0.02 a.u.) for the main components of the electronic transitions of compound **6**.

In contrast, for the second excitation, which involves transitions from the HOMO – 2 and HOMO – 3 orbitals, there is amplitude on carbon C₇. The conjugation between the orbitals involved in the transition is higher in the latter case than in the former case.

The selected bond lengths obtained from the optimised structure for the ground state (GS) and excited state (ES) forms of compound **6** are presented in Table S7 (see ESI[†]). A comparison of the GS and ES structures reveals that, in the excited state, the double-bond length C₇–C₈ (see ESI[†], Table S7; atom labels are shown on the top of Fig. 7) increases from 1.373 to 1.416 Å (3.1%). Several bonds in the phenyl ring also increase in length, most notably C₂–C₃ (0.038 Å; 2.74%) and C₁–C₆ (0.027 Å; 1.9%). In contrast, the C₁–C₂ (–0.022 Å; –1.49%) and C₆–O₁₁ (–0.019 Å; –1.40%) bond lengths decrease. The calculated structural changes for the excited state are consequences of the electronic transitions that occur during the excitation process, as indicated by the HOMO and LUMO surfaces (Fig. 8). The transition from the HOMO (the e_{1g} bonding orbital of the phenyl ring) to the LUMO (an antibonding orbital that is primarily located on the methylene group) results in an increase in the C₇–C₈ bond length. In addition, as shown in Fig. 8, the C₆–O₁₁ bond possesses an antibonding character in the occupied orbitals. Therefore, a HOMO–LUMO electron transfer results in a decrease in the C₆–O₁₁ bond length. One additional consequence of the excitation process is a decrease in the electronic charge densities on O₁₁ and C₁ and an increase in the negative charge on C₇ (see ESI[†], Table S9).

To help rationalise the reduction process, geometry optimisations at the B3LYP/6-31+G(d,p) level were performed for one electron reduction in a vacuum and CH₂Cl₂, using the PCM solvation model.^{39,40} The diffuse functions were added to appropriately describe the resulting anions. Geometrical parameters for the first reduced form are also given in Table S7 (see ESI[†]). The geometries found for the anions are similar to the geometry of the neutral form. The charge and spin densities for the one-electron reduced form are provided in Table S9 (see ESI[†]). The spin densities for the gas phase geometries show a symmetrical distribution of the spin densities between the two dicyanomethylene moieties (see ESI[†], Fig. S27 and S28). In contrast, calculation in the solvent promotes the localization of the spin density in one side (see ESI[†], Fig. S27 and S28). Most likely this difference may be related to the polarization of the molecules promoted by the solvent. In both phases the spin density distribution in the reduced form follows a pattern very similar to that found for the LUMOs (Fig. 8 and see ESI[†], Fig. S28), with spin concentration on the C₇ and C₈ carbon atoms, and some polarisation to the aromatic ring and the nitrile groups. This result clearly indicates that the methylene moiety controls both the spectroscopic features and the electrochemistry of the examined compounds.

Conclusions

The five new dicyanomethylene compounds characterised in the present study possess interesting structural, spectroscopic

and electrochemical properties. X-ray single-crystal structure analyses of **5**, **10**, **11** and **12** revealed that the 3D crystal packing for all of the examined structures is governed by a number of weak hydrogen bonds. The compounds containing an odd number of atoms in the spacer (**5** and **11**) revealed a V-shaped arrangement of the phenyl rings and the compounds containing an even number of atoms in the spacer (**6**, **10** and **12**) showed a parallel arrangement of the phenyl rings. All synthesised compounds showed blue emissions in the solid state and in solution. Stokes shift range from 0.51 to 0.58 eV in solution. Compound **10**, with the shortest spacer, exhibited the highest Stokes shift in the solid state, 0.68 eV, suggesting that this compound might be experiencing a larger geometry change upon excitation.

The electronic transitions for the synthesized compounds in solution could be assigned on the basis of DFT calculations and revealed that the main transitions involve the e_{1g} orbital of the phenyl ring (HOMO) and the double bonds of the methylenic group (LUMO). These electronic transitions influence both the geometrical and electronic properties of the groups involved in the transitions. The electronic transitions observed in the solid state most likely involve the same orbitals considering the similar patterns of the spectra in solution and in the solid state. TD-DFT simulations of the emission spectra indicate that the fluorescence of these compounds originates from electronic transitions from the aromatic system of the methoxyphenyl moiety to the adjacent propanedinitrile group. The simulation of the electrochemical process in solution demonstrated that the one-electron reduction involves only one of the [(2-methoxyphenyl)methylene]propanedinitrile fragments.

Experimental

All of the chemicals used in this study were purchased from Aldrich and were used without further purification. Solvents were purchased from Vetec (Brazil) and were purified according to procedures in the extant literature. Thin-layer chromatography (TLC) was performed on aluminium sheets coated with silica gel 60F (Merck 5554). The plates were inspected under UV light and, if necessary, developed in I₂ vapour. Column chromatography was performed on silica gel 60 (Merck; 40–60 nm, 230–400 mesh). Melting points were determined on a Thermo Scientific 9100 and were reported without corrections. Infrared spectra were recorded on a Perkin Elmer FT-IR spectrometer using KBr pellets. ¹H and ¹³C NMR spectra were recorded on a Bruker instrument (at 500 and 125 MHz, respectively), using residual solvents as internal standards. Samples were prepared using CDCl₃ purchased from Cambridge Isotope Laboratories. Elemental analyses were conducted on a Perkin Elmer CHN 2400 analyser at the Central Analítica of the Instituto de Química at the Universidade de São Paulo in Brazil.

Absorption and emission spectroscopy

Absorption spectra were obtained on a Cary 50 spectrophotometer using spectroscopic-grade CH₂Cl₂. The photoluminescence (PL) spectroscopy measurements were carried out at room

temperature using a Photon Technology International (PTI) fluorescence spectrophotometer. Diffuse Reflectance UV-Visible spectra (DR UV-Vis) were recorded using a Varian Cary 5000 spectrometer using Cary win-UV/scan software. Fluorescence quantum yields were determined using a quinine bisulphate (QB) solution in 0.5 M H₂SO₄ ($\Phi = 0.546$)⁴¹ as a reference material. The quantum yield was determined using the following equation:^{42,43}

$$\Phi_{\text{em,S}} = \Phi_{\text{em,R}} (f_{\text{R}}/f_{\text{S}})(I_{\text{S}}/I_{\text{R}})(n_{\text{S}}/n_{\text{R}})$$

where $\Phi_{\text{em,S}}$ represents the fluorescence quantum yield of the sample; f_{S} and f_{R} are the absorption factors ($f = 1 - 10^{-\text{Abs}}$, where Abs = absorbance) for the sample and the reference, respectively, at the excitation wavelength; I_{S} and I_{R} denote the integrated areas of the corrected emission spectra for the sample and the reference, respectively; and n_{S} and n_{R} are the refractive indices of the sample and reference solvents, respectively.

All fluorescence lifetime measurements were carried out in a homemade laser table. A quartz cuvette (10 mm pathlength) containing a solution of the dicyanomethylene compounds at the concentration of 10^{-5} mol dm⁻³ was irradiated using a third harmonic (355 nm, 185 mJ) Nd-YAG pulsed laser (Quantel BRILLIANT-B). The emissions were collected at 90° to the excitation on an Oriel Cornerstone™ 260 1/4 m monochromator at the selected wavelengths (440 nm) and detected using a PMT (Oriel 77360, risetime = 1.2 ns). The signals were captured using an oscilloscope (LeCroy Wavesurfer 44MXs-B, 400 MHz).

Single crystal structure determination

Single crystals of **5**, **10**, **11**, and **12** that were suitable for X-ray diffraction experiments were obtained by the slow evaporation of solutions of these compounds (at 1.0 mmol dm⁻³) in CH₂Cl₂/C₆H₆. X-ray diffraction data were collected on an Oxford Diffraction Gemini diffractometer using a graphite-enhanced source of MoK α radiation ($\lambda = 0.7107$ Å) for compounds **10**, **11** and **12** and an enhanced source of CuK α radiation ($\lambda = 1.5418$ Å) for compound **5**. The data integration and scaling of the reflections for all of the compounds were performed using the *Chrysalis* software suite.⁴⁴ The final unit-cell parameters were based on the fitting of all of the reflection positions. Analytical⁴⁵ and semi-empirical⁴⁶ absorption corrections were performed using the *Chrysalis* software suite.⁴⁴ The *XPREF*⁴⁷ program was used for space-group identification. The structures of all of the examined compounds were solved by direct methods using the *SHELXS*⁴⁷ software program. The positions of all of the atoms could be unambiguously assigned on consecutive difference Fourier maps. No solvent molecules were observed in the structures of the assessed compounds. *SHELXL*⁴⁷ was used to apply a full-matrix least-squares approach to perform refinements that were based on F^2 . All of the hydrogen atoms were refined with anisotropic atomic displacement parameters. The hydrogen atoms in the compounds were added to the structure in idealised positions and were further refined according to a riding model.⁴⁸

All single-crystal samples of compounds **5** and **11** were merohedrally twinned, *i.e.*, the complete superpositions of all of the reflections in the reciprocal space were caused by the

existence of two domains that were related by a non-crystallographic lattice rotation. Because the single crystals are described by monoclinic symmetry, this rare case is only possible for particular combinations of lattice parameters and monoclinic angles. The details regarding the refinement of these monoclinic samples will be published elsewhere.

Electrochemistry

Cyclic voltammetric (CV) experiments were performed in argon-purged CH₂Cl₂ (Aldrich) at room temperature using a micro Autolab Type III system that was interfaced with a personal computer. A glassy carbon working electrode was utilised for these experiments, and its surface was polished with 0.3 μm alumina-water slurry on a felt surface prior to each use. The counter electrode was a Pt wire that was separated from the bulk solution by a fine glass frit, and the reference for these experiments was an Ag/AgCl electrode in organic media. Ferrocene was used as an internal standard ($E_{1/2}$ of 0.40 V vs. NHE). Under all of the tested conditions, the concentration of each compound was 6.6×10^{-4} mol dm⁻³, and 0.1 mol dm⁻³ tetrabutylammonium perchlorate (TBAClO₄, Fluka) was added to the solutions as a supporting electrolyte. Cyclic voltammograms were obtained at sweep rates in the range of 0.02–1.0 V s⁻¹.

Theoretical calculations

DFT calculations were performed using the Gaussian 09 (Rev. B.01) software package.⁴⁹ All geometries were fully optimized starting from two initial arrangements, one using the geometry obtained in the solid state measurements and the second one starting from a fully planar geometry, with the spacer chain in a zig-zag arrangement. For the geometry optimization calculation the B3LYP functional together with the 6-31G(d,p) basis set was employed.^{50,51}

Harmonic frequency calculations were performed for the optimised geometries and revealed that these geometries represent genuine minimum energy points (with no negative eigenvalue) on the potential energy surface. Based on the B3LYP/6-31G(d,p) optimised geometries, TD-DFT approaches were used to simulate vertical excitations with linear responses to verify the effects of these excitations on the absorption spectra of the examined compounds.

The polarised continuum (overlapping spheres) solvation model (PCM) was used to ensure that solvent effects (CH₂Cl₂) were incorporated into all of the aforementioned calculations. The PCM computations used the UFF radii and all of the standard specifications of the Gaussian package. The thermodynamic calculations in solution were performed as described by Pliego and Riveros⁵² using the Gibbs free energy of solvation as described by Ben-Naim.⁵³ All values reported are those obtained in solution (CH₂Cl₂).

The photophysical properties of compound **6** were explored in detail. The geometry of the first excited state was optimized, followed by frequency calculations. This procedure permitted a Franck-Condon analysis^{54,55} and the generation of simulated emission spectra. State-specific^{56,57} TD-DFT was performed at the ground- and excited-state geometries to obtain a more

accurate emission value that corresponded to the S1 \rightarrow S0 transition. The emission band shape was calculated using FC analysis parameters of a half-width at half-maximum (HWHM) of 2000 cm^{-1} and a spectral resolution of 1 cm^{-1} .

To evaluate the orbitals that are involved in the electronic transitions, a NTO analysis was performed for compound **6**. The TD results were analysed using the GaussSum software.⁵⁸ The absorption spectra were fitted with a Gaussian function with a FWHM of 3000 cm^{-1} .

Synthesis

Compound 3. The synthesis of compound **3** has been described elsewhere.⁵⁹

Compound 4. The synthesis of compound **4** was analogous to the synthesis of **3**, using **2** (1.50 g, 3.27 mmol), salicylic aldehyde (0.957 g, 7.85 mmol) and K_2CO_3 (2.16 g, 15.70 mmol) in dry MeCN (80 mL). After the reaction mixture was cooled to room temperature, the solid was filtered away, and the solvent was removed under vacuum. The residue was purified by column chromatography (SiO_2 ; hexane : EtOAc 1 : 1) to produce the desired product (0.850 g, 73% yield) as a light-yellow solid with the following properties: m.p.: 44–46 $^\circ\text{C}$. ^1H NMR (500 MHz, CDCl_3) δ : 10.50 (s, 2H), 7.81 (dd, $J = 8.0$ Hz and $J = 2.0$ Hz, 2H), 7.53–7.50 (m, 2H), 7.03–6.97 (m, 4H), 4.24 (t, $J = 4.5$ Hz, 4H), 3.91 (t, $J = 4.5$ Hz, 4H) and 3.74 (s, 4H). ^{13}C NMR (125 MHz, CDCl_3) δ : 190.1, 161.4, 136.1, 128.5, 125.3, 121.1, 113.0, 71.2, 69.8 and 68.4. IR (KBr) $\nu(\text{cm}^{-1})$: 2924.51(w), 2869.20(w), 2761.22(w), 1678.74(s), 1599.72(s), 1481.20(m), 1453.55(m), 1391.65(w), 1348.20(w), 1287.62(s), 1240.21(s), 1184.90(w), 1105.89(s), 1042.68(m), 916.26(w), 829.34(m), 758.23(s), 647.61(m) and 598.89(w). Elemental analysis for $\text{C}_{20}\text{H}_{22}\text{O}_6$: calculated: 67.07% C and 6.19% H; experimentally determined: 66.94% C and 6.08% H.

Compound 5. A mixture of **3** (0.996 g, 3.13 mmol), $\text{CH}_2(\text{CN})_2$ (0.500 g, 7.82 mmol) and NH_4OAc (0.0024 g, 0.03 mmol) was ground in a mortar. The product was purified by column chromatography (SiO_2 , CH_2Cl_2) to generate a yellow solid (1.00 g, 78% yield) with the following properties: m.p.: 148–150 $^\circ\text{C}$. ^1H NMR (500 MHz, CDCl_3) δ : 8.28 (s, 2H), 8.18 (dd, $J = 8.0$ Hz and $J = 1.0$ Hz, 2H), 7.58–7.55 (m, 2H), 7.1 (t, $J = 8.0$ Hz, 2H), 7.01 (d, $J = 8.5$ Hz, 2H), 4.27 (t, $J = 4.5$ Hz, 4H) and 3.96 (t, $J = 4.5$ Hz, 4H). ^{13}C NMR (125 MHz, CDCl_3) δ : 158.0, 154.3, 136.4, 128.7, 121.6, 120.4, 114.2, 112.7, 81.4, 69.4 and 68.4. IR (KBr) $\nu(\text{cm}^{-1})$: 3039(w), 2953(w), 2933(w), 2226(m), 1601(s), 1582(s), 1484(s), 1262(s), 1139(m) and 748(s). Elemental analysis for $\text{C}_{24}\text{H}_{18}\text{O}_3\text{N}_4$: calculated: 70.23% C, 4.42% H and 13.65% N; experimentally determined: 69.84% C, 3.94% H and 13.60% N.

Compound 6. The synthesis of **6** was analogous to the synthesis of **5** using **4** (0.850 g, 2.4 mmol), $\text{CH}_2(\text{CN})_2$ (0.634 g, 9.6 mmol) and NH_4OAc (0.740 g, 9.6 mmol). A yellow solid was obtained after purification (0.792 g, 74% yield) that possessed the following properties: m.p.: 149–151 $^\circ\text{C}$. ^1H NMR (500 MHz, CDCl_3) δ : 8.31(s, 2H), 8.16 (dd, $J = 8.0$ Hz and $J = 1.5$ Hz, 2H), 7.58–7.54 (m, 2H), 7.08 (t, $J = 8.0$ Hz, 2H), 6.7 (d, $J = 8.5$ Hz, 2H), 4.24 (t, $J = 4.5$ Hz, 4H), 3.90 (t, $J = 5.0$ Hz, 4H) and 3.76 (s, 4H).

^{13}C NMR (125 MHz, CDCl_3) δ : 158.5, 154.7, 136.7, 128.9, 121.8, 120.7, 114.6, 113.1, 81.5, 71.0, 69.5 and 68.7. IR (KBr) $\nu(\text{cm}^{-1})$: 3043(w), 2970(w), 2916(w), 2221(m), 1600(m), 1579(s), 1480(m), 1462(m), 1367(m), 1257(s), 1137(s) and 751(m). Elemental analysis for $\text{C}_{26}\text{H}_{22}\text{O}_4\text{N}_4$: calculated: 68.71% C, 4.88% H and 12.33% N; experimentally determined: 67.56% C, 4.62% H and 11.70% N.

Compound 7. A mixture of salicylic aldehyde (8.00 g, 65.5 mmol), K_2CO_3 (9.00 g, 65.5 mmol), KI (5.66 g, 26.20 mmol) and 1,4-dibromobutane (5.66 g, 26.204 mmol) in dry MeCN (50 mL) was heated for 12 h under reflux. After the reaction mixture was cooled to room temperature, the solid was filtered away, and the solvent was removed under vacuum. The residue was then dissolved in CH_2Cl_2 and washed with cold water and saturated brine. After this solution was dried over anhydrous sodium sulphate, the solvent was removed under reduced pressure to produce the desired product in the form of pale crystals (3.26 g, 40.8% yield). m.p.: 112–116 $^\circ\text{C}$. ^1H NMR (500 MHz, CDCl_3) δ : 10.5 (s, 2H), 7.82 (dd, $J = 7.5$ and 1.5 Hz, 2H), 7.56–7.52 (m, 2H), 7.04–6.97 (m, 4H), 4.19 (t, $J = 5.5$ Hz, 4H) and 2.11–2.09 (m, 4H). ^{13}C NMR (125 MHz, CDCl_3) δ : 189.3, 161.0, 135.8, 128.3, 124.7, 120.6, 112.2, 67.7 and 25.7. IR (KBr) $\nu(\text{cm}^{-1})$: 3107(w), 3078(w), 2952(m), 2876(m), 2759(w), 1679(s), 1595(w), 1493(s), 1461(s), 1382(s), 1287(s), 1237(s), 1195(m), 1145(m), 1006(m), 846(s), 754(s), 657(m) and 609(m). Elemental analysis for $\text{C}_{18}\text{H}_{18}\text{O}_4$: calculated: 72.47% C and 6.08% H; experimentally determined: 73.43% C and 6.29% H.

Compound 8. The synthesis of **8** was analogous to the synthesis of **7** using 1,5-dibromopentane (1.51 g, 6.56 mmol), salicylic aldehyde (2.00 g, 16.4 mmol), K_2CO_3 (2.26 g, 16.4 mmol) and KI (2.18 g, 13.1 mmol) in dry MeCN (50 mL). Pale crystals were obtained after the solvent was removed under reduced pressure (2.38 g, 90% yield). m.p.: 54.6 $^\circ\text{C}$. ^1H NMR (500 MHz, CDCl_3) δ : 10.48 (s, 2H), 7.80 (dd, $J = 7.5$ and 2.0 Hz, 2H), 7.53–7.49 (m, 2H), 7.03–6.97 (m, 4H), 4.10 (t, $J = 6.5$ Hz, 4H), 1.97–1.91 (m, 4H) and 1.74–1.67 (m, 2H). ^{13}C NMR (125 MHz, CDCl_3) δ : 189.54, 161.18, 135.79, 128.23, 124.76, 120.50, 112.33, 68.08, 28.70 and 22.66. IR (KBr) $\nu(\text{cm}^{-1})$: 2949(w), 2868(w), 1678(s), 1480(m), 1459(s), 1460(m), 1292(m), 1240(s), 1185(w), 1155(m), 1112(w), 1076(w), 1011(w), 1008(m), 984(w), 917(w), 839(m), 764(s) and 656(m). Elemental analysis for $\text{C}_{19}\text{H}_{20}\text{O}_4$: calculated: 73.06% C and 6.45% H; experimentally determined: 73.22% C and 6.74% H.

Compound 9. The synthesis of **9** was analogous to the syntheses of **7** and **8** using 1,6-dibromohexane (6.39 g, 26.20 mmol), salicylic aldehyde (8.00 g, 65.5 mmol), K_2CO_3 (9.04 g, 65.50 mmol) and KI (8.60 g, 52.4 mmol) in dry MeCN (50 mL). Pale crystals were obtained after the solvent was removed under reduced pressure (7.24 g, 67% yield). m.p.: 76.6 $^\circ\text{C}$. ^1H NMR (500 MHz, CDCl_3) δ : 10.51 (s, 2H), 7.83 (dd, $J = 7.5$ and 1.5 Hz, 2H), 7.55–7.52 (m, 2H), 7.03–6.97 (m, 4H), 4.10 (t, $J = 6.5$ Hz, 4H), 1.93–1.88 (m, 4H) and 1.62–1.59 (m, 4H). ^{13}C NMR (125 MHz, CDCl_3) δ : 189.6, 158.3, 154.2, 136.47, 128.7, 125.0, 121.1, 112.17, 68.6, 68.3, 28.7 and 25.7. IR (KBr) $\nu(\text{cm}^{-1})$: 3072(w); 2955(w), 2933(w), 2850(w), 2760(w), 1685(s), 1602(s), 1486(m), 1459(s), 1395(m), 1291(s), 1246(s), 1164(w), 1110(w),

1081(w), 1037(w), 999(w), 833(m) and 758(m). Elemental analysis for $C_{20}H_{22}O_4$: calculated: 73.60% C and 6.79% H; experimentally determined: 73.40% C and 7.00% H.

Compound 10. 7 (2.00 g, 6.7 mmol), $CH_2(CN)_2$ (1.32 g, 20 mmol) and $AcONH_4$ (1.54 g, 20 mmol) were mixed. A yellow solid was obtained after purification (0.785 g, 30% yield). m.p.: 212–215 °C. 1H NMR (500 MHz, DMSO) δ : 8.19 (s, 2H), 8.17 (dd, $J = 8.0$ and 1.0 Hz, 2H), 7.59–7.55 (m, 2H), 7.06 (t, $J = 8.0$ Hz, 2H), 6.96 (d, $J = 8.5$ Hz, 2H), 4.17 (t, $J = 5.0$ Hz, 4H) and 2.07–2.06 (m, 4H). ^{13}C NMR (125 MHz, DMSO) δ : 156.7, 154.4, 128.5, 128.1, 120.2, 114.3, 113.1, 87.2, 68.4 and 25.0. IR (KBr) ν (cm^{-1}): 3039(w), 2949(w), 2888(w), 2224(m), 1598(m), 1578(m), 1485(m), 1454(m), 1392(w), 1365(m), 1312(m), 1256(s), 1200(w), 1156(m), 1042(m), 980(m), 751(m) and 616(w). Elemental analysis for $C_{24}H_{18}O_2N_4$: calculated: 73.08% C, 4.60% H and 14.20% N; experimentally determined: 72.54% C, 4.70% H and 14.05% N.

Compound 11. The synthesis of **11** was analogous to the syntheses of **5**, **6** and **10** using **8** (0.290 g, 0.9 mmol), $CH_2(CN)_2$ (0.182 g, 2.76 mmol), and $AcONH_4$ (0.213 g, 2.7 mmol). A yellow solid was obtained after purification (0.172 g, 46% yield). m.p.: 178 °C. 1H NMR (500 MHz, $CDCl_3$) δ : 8.29 (s, 2H), 8.20 (dd, $J = 8.0$ Hz and 1.5 Hz, 2H), 7.59–7.55 (m, 2H), 7.08 (t, $J = 7.5$ Hz, 2H), 6.99 (d, $J = 8.5$ Hz, 2H), 4.13 (t, $J = 6.5$ Hz, 4H), 1.98 (m, 4H) and 1.68 (m, 2H). ^{13}C NMR (125 MHz, $CDCl_3$) δ : 158.2, 154.2, 136.4, 128.8, 120.1, 114.3, 112.8, 112.16, 81.3, 68.5, 28.6 and 22.7. IR (KBr) ν (cm^{-1}): 3041(w), 2957(w), 2934(w), 2222(m), 1581(m), 1483(m), 1478(w), 1456(w), 1389(m), 1367(w), 1309(w), 1262(s), 1168(w), 1100(w), 1059(w), 1019(w), 987(w) and 743(s). Elemental analysis for $C_{25}H_{20}O_2N_4$: calculated: 73.51% C, 4.94% H and 13.72% N; experimentally determined: 73.47% C, 5.07% H and 13.59% N.

Compound 12. **9** (5.06 g, 15.5 mmol), $CH_2(CN)_2$ (3.07 g, 46.5 mmol) and $AcONH_4$ (3.59 g, 46.5 mmol) were mixed. A yellow solid was obtained after purification (4.20 g, 64% yield). m.p.: 169 °C. 1H NMR (500 MHz, $CDCl_3$) δ : 8.26 (s, 2H), 8.18 (dd, $J = 7.8$ and 1.5 Hz, 2H), 7.59–7.53 (m, 2H), 7.06 (t, $J = 7.5$ Hz, 2H), 6.97 (d, $J = 8.4$ Hz, 2H), 4.09 (t, $J = 6.3$ Hz, 4H), 1.91–1.86 (m, 4H) and 1.60–1.58 (m, 4H). ^{13}C NMR (125 MHz, $CDCl_3$) δ : 158.2, 154.1, 136.4, 128.4, 121.0, 114.3, 112.8, 112.2, 81.0, 68.6, 28.7 and 25.6. IR (KBr) ν (cm^{-1}): 3034(w), 2952(w), 2944(w), 2854(w), 2225(m), 1598(m), 1578(m), 1485(m), 1447(m), 1388(w), 1358(w), 1309(m), 1258(s), 1156(m), 993(m) and 750(s). Elemental analysis for $C_{26}H_{22}O_2N_4$: calculated: 73.92% C, 5.25% H and 13.26% N; experimentally determined: 73.91% C, 5.40% H and 13.13% N.

Acknowledgements

The authors gratefully acknowledge FAPERJ (JCNE grant number E-26/103.213/2011 and Pensa Rio grant number E-26/110.692/2012) and CNPq (the C.R.M.O. Matos fellowship and Universal grant number 478302/2012-6) for financial support. C.M.R., J.W.M.C. and C.B.P. are recipients of CNPq research fellowships. We thank Dr E. A. Ponzio (IQ-UFF, Brazil) for assistance with the cyclic voltammetry experiments and

Dr Marco Cremona (IF-PUC, Rio de Janeiro, Brazil) for PL spectroscopy measurements.

Notes and references

- N. A. J. M. Sommerdijk, *Angew. Chem., Int. Ed.*, 2003, **42**, 3572.
- J.-P. Zhang, Y.-B. Zhang, J.-B. Lin and X.-M. Chen, *Chem. Rev.*, 2012, **112**, 1001.
- A. Schoedel, L. Wojtas, S. P. Kelley, R. D. Rogers, M. Eddaoudi and M. J. Zaworotko, *Angew. Chem., Int. Ed.*, 2011, **50**, 11421.
- B. J. Holliday and C. A. Mirkin, *Angew. Chem., Int. Ed.*, 2001, **40**, 2022.
- P. J. Stang and B. Olenyuk, *Acc. Chem. Soc.*, 1997, **30**, 502.
- D. L. Caulder and K. N. Raymond, *J. Chem. Soc., Dalton Trans.*, 1999, 1185.
- M. Albrecht, *Chem. Soc. Rev.*, 1998, **27**, 281.
- O. M. Yaghi, M. O'Keeffe, N. W. Ockwig, H. K. Chae, M. Eddaoudi and J. Kim, *Nature*, 2003, **423**, 705.
- S. Subramanian and M. J. Zaworotko, *Angew. Chem., Int. Ed. Engl.*, 1995, **34**, 2127.
- Y.-B. Dong, Y.-Y. Jiang, J. Li, J.-P. Ma, F.-L. Liu, B. Tang, R.-Q. Huang and S. R. Batten, *J. Am. Chem. Soc.*, 2007, **129**, 4521.
- H.-J. Kim, W.-C. Zin and M. Lee, *J. Am. Chem. Soc.*, 2004, **126**, 7009.
- A. S. Abd-El-Aziz and E. A. Strohmb, *Polymer*, 2012, **53**, 4879.
- G. K. Patra and I. Goldberg, *Cryst. Growth Des.*, 2003, **3**, 321.
- Q. Yang, X. Chen, Z. Chen, Y. Hao, Y. Li, Q. Lu and H. Zheng, *Chem. Commun.*, 2012, **48**, 10016.
- L.-F. Ma, X.-Q. Li, Bin-Liu, L.-Y. Wang and H.-W. Hou, *CrystEngComm*, 2011, **13**, 4973.
- S. Konar, P. S. Mukherjee, M. G. B. Drew, J. Ribas and N. R. Chaudhuri, *Inorg. Chem.*, 2003, **42**, 2545.
- R. J. Angelici, M. H. Quick, G. A. Kraus and D. T. Plummer, *Inorg. Chem.*, 1982, **21**, 2178.
- V. E. de Oliveira, R. Diniz and L. F. C. de Oliveira, *Quim. Nova*, 2009, **32**, 1917.
- L. Carlucci, G. Ciani, P. Macchi, D. M. Proserpio and S. Rizzato, *Chem.-Eur. J.*, 1999, **5**, 237.
- C. T. Imrie and P. A. Henderson, *Chem. Soc. Rev.*, 2007, **36**, 2096.
- H. Qu, L. Qiu, X.-K. Leng, M.-M. Wang, S.-M. Lan, L.-L. Wen and D.-F. Li, *Inorg. Chem. Commun.*, 2011, **14**, 1347.
- L. Shi, Z. Liu, G. Dong, L. Duan, Y. Qiu, J. Jia, W. Guo, D. Zhao, D. Cui and X. Tao, *Chem.-Eur. J.*, 2012, **18**, 8092.
- E. V. Anslyn and D. A. Dougherty, *Modern Physical Organic Chemistry*, University Science Books, Sausalito, CA, 2006.
- R. R. Gagné, C. A. Koval and G. C. Lisensky, *Inorg. Chem.*, 1980, **19**, 2854.
- V. V. Pavlishchuk and A. W. Addison, *Inorg. Chim. Acta*, 2000, **298**, 97.
- Y. Liu, M. S. Liu and A. K.-Y. Jen, *Acta Polym.*, 1999, **50**, 105.
- S. C. Chang and M. J. Weaver, *J. Phys. Chem.*, 1991, **95**, 5391.

- 28 E. M. Stuve, A. Krasnopoler and D. E. Sauer, *Surf. Sci.*, 1995, **335**, 177.
- 29 L. L. Miller, G. D. Nordbloman and E. A. Maybda, *J. Org. Chem.*, 1972, **37**, 916.
- 30 P. Pösch, M. Thelakkat and H. W. Schmidt, *Synth. Met.*, 1999, **102**, 1110.
- 31 J. Pommerehne, H. Vestweber, W. Guss, R. F. Mahrt, H. Bassler, M. Porsch and J. Daub, *Adv. Mater.*, 1995, **7**, 551.
- 32 A. D. Becke, *J. Chem. Phys.*, 1993, **98**, 5648.
- 33 R. Ditchfield, W. J. Hehre and J. A. Pople, *J. Chem. Phys.*, 1971, **54**, 724.
- 34 A. Dreuw and M. Head-Gordon, *J. Am. Chem. Soc.*, 2004, **126**, 4007.
- 35 A. Dreuw and M. Head-Gordon, *Chem. Rev.*, 2005, **105**, 4009.
- 36 R. Bauernschmitt and R. Ahlrichs, *Chem. Phys. Lett.*, 1996, **256**, 454.
- 37 F. Furche and R. Ahlrichs, *J. Chem. Phys.*, 2002, **117**, 7433.
- 38 R. L. Martin, *J. Chem. Phys.*, 2003, **118**, 4775.
- 39 S. Miertuš, E. Scrocco and J. Tomasi, *Chem. Phys.*, 1981, **55**, 117.
- 40 J. Tomasi, B. Mennucci and R. Cammi, *Chem. Rev.*, 2005, **105**, 2999.
- 41 G. F. Kirkbright, *Anal. Chem.*, 1977, **49**, 1850.
- 42 J. B. Birks, *Photophysics of Aromatic Molecules*, Wiley-Interscience, London, 1st edn, 1970.
- 43 A. M. Brouwer, *Pure Appl. Chem.*, 2011, **83**, 2213.
- 44 Agilent Technologies, *Xcalibur CCD system, CrysAlisPro Software system, Version 1.171.35.21*, Agilent Technologies UK Ltd., Oxford, UK, 2011.
- 45 Analytical numeric absorption correction using a multi-faceted crystal model based on expressions derived by R. C. Clark and J. S. Reid. (R. C. Clark and J. S. Reid, *Acta Crystallogr., Sect. A: Fundam. Crystallogr.*, 1995, **51**, 887).
- 46 Empirical absorption correction using spherical harmonics, implemented in the SCALE3 ABSPACK scaling algorithm.
- 47 G. M. Sheldrick, *Acta Crystallogr., Sect. A: Fundam. Crystallogr.*, 2008, **64**, 112.
- 48 C. K. Johnson, in *Crystallographic Computing*, ed. F. R. Ahmed, Munksgaard, Copenhagen, 1970, pp. 207–219.
- 49 M. J. Frisch, G. W. Trucks, H. B. Schlegel, G. E. Scuseria, M. A. Robb, J. R. Cheeseman, G. Scalmani, V. Barone, B. Mennucci, G. A. Petersson, H. Nakatsuji, M. Caricato, X. Li, H. P. Hratchian, A. F. Izmaylov, J. Bloino, G. Zheng, J. L. Sonnenberg, M. Hada, M. Ehara, K. Toyota, R. Fukuda, J. Hasegawa, M. Ishida, T. Nakajima, Y. Honda, O. Kitao, H. Nakai, T. Vreven, J. A. Montgomery Jr., J. E. Peralta, F. Ogliaro, M. Bearpark, J. J. Heyd, E. Brothers, K. N. Kudin, V. N. Staroverov, R. Kobayashi, J. Normand, K. Raghavachari, A. Rendell, J. C. Burant, S. S. Iyengar, J. Tomasi, M. Cossi, N. Rega, J. M. Millam, M. Klene, J. E. Knox, J. B. Cross, V. Bakken, C. Adamo, J. Jaramillo, R. Gomperts, R. E. Stratmann, O. Yazyev, A. J. Austin, R. Cammi, C. Pomelli, J. W. Ochterski, R. L. Martin, K. Morokuma, V. G. Zakrzewski, G. A. Voth, P. Salvador, J. J. Dannenberg, S. Dapprich, A. D. Daniels, Ö. Farkas, J. B. Foresman, J. V. Ortiz, J. Cioslowski and D. J. Fox, *Gaussian 09, Revision B.01*, Gaussian, Inc., Wallingford, CT, 2009.
- 50 A. D. Becke, *J. Chem. Phys.*, 1993, **98**, 5648.
- 51 R. Ditchfield, W. J. Hehre and J. A. Pople, *J. Chem. Phys.*, 1971, **54**, 724.
- 52 J. R. Pliego and J. M. Riveros, *Phys. Chem. Chem. Phys.*, 2002, **4**, 1622.
- 53 A. Ben-Naim, *J. Phys. Chem.*, 1978, **82**, 792.
- 54 F. Santoro, A. Lami, R. Improta, J. Bloino and V. Barone, *J. Chem. Phys.*, 2008, **128**, 224311.
- 55 M. Dierksen and S. Grimme, *J. Phys. Chem. A*, 2004, **108**, 10225.
- 56 R. Improta, V. Barone, G. Scalmani and M. J. Frisch, *J. Chem. Phys.*, 2006, **125**, 054103.
- 57 R. Improta, G. Scalmani, M. J. Frisch and V. Barone, *J. Chem. Phys.*, 2007, **127**, 074504.
- 58 N. M. O'Boyle, A. L. Tenderholt and K. M. Langner, *J. Comput. Chem.*, 2008, **29**, 839.
- 59 N. C. F. Dionysio, J. Bordinhão, L. C. Visentin and C. M. Ronconi, *Acta Crystallogr., Sect. E: Struct. Rep. Online*, 2008, **64**, o546.